Electronic Supplementary Material (ESI) for Journal of Materials Chemistry A.

Supporting Information

Homogeneous Li deposition through the control of carbon dot assisted Li dendrite morphology for high-performance Li metal batteries

Dongki Hong,[a] Yuri Choi,[b] Jaegeon Ryu,[c] Jinhong Mun,[b] Wooyeong Choi,[a] Minju Park,[a] Yongwon Lee,[a] Nam-Soon Choi,[a] Geunsik Lee,[b] Byeong-Su Kim,[d]* Soojin Park[c]**

[a]School of Energy and Chemical Engineering, Ulsan National Institute of Science and Technology (UNIST), 50 UNIST-gil, Ulsan 44919, Republic of Korea

[b]Department of Chemistry, School of Natural Science, Ulsan National Institute of Science and Technology (UNIST), 50 UNIST-gil, Ulsan 44919, Republic of Korea

[c]Department of Chemistry, Division of Advanced Materials Science, Pohang University of Science and Technology (POSTECH), 77 Cheongam-Ro, Pohang 37673, Republic of Korea

[d]Department of Chemistry, Yonsei University, 50 Yonsei-ro, Seoul 03722, Republic of Korea

*Corresponding Author

Soojin Park (soojin.park@postech.ac.kr)

Department of Chemistry, Division of Advanced Materials Science, Pohang University of Science and Technology (POSTECH), 77 Cheongam-Ro, Pohang 37673, Republic of Korea
Tel. +82-54-279-2102,

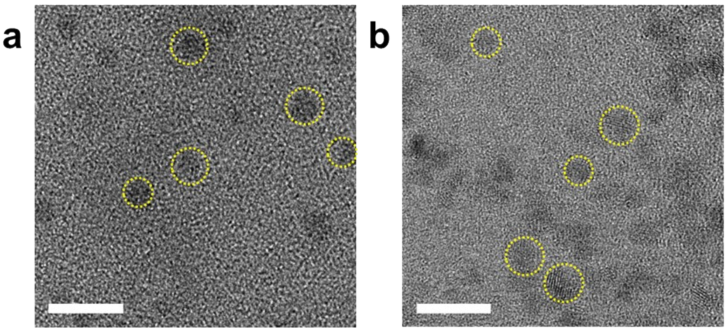

Figure S1. TEM images of as-synthesized carbon dots. (a) U-CD. (b) N-CD. Scale bars are 10 nm.

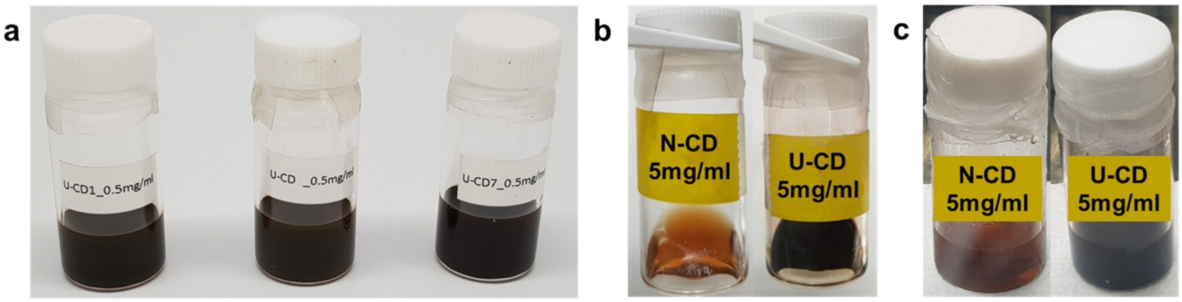

Figure S2. Photographs of the dispersed CDs in carbonate electrolyte. (a) U-CD variations with 0.5 mg mL^{-1} electrolyte concentration. (b) N-CD and U-CD with 5 mg mL^{-1} electrolyte concentration. (c) Electrolyte stability of the N-CD and U-CD after six months. To further investigate the effect of the surface charge and functional groups of the U-CD, variation samples of U-CD1 and U-CD7 were designed. For the preparation of U-CD1 and U-CD7, 1 mmol and 7 mmol of citric acid was dissolved in 10 mL of DMF, respectively. Other synthetic steps were identical to the U-CD preparation.

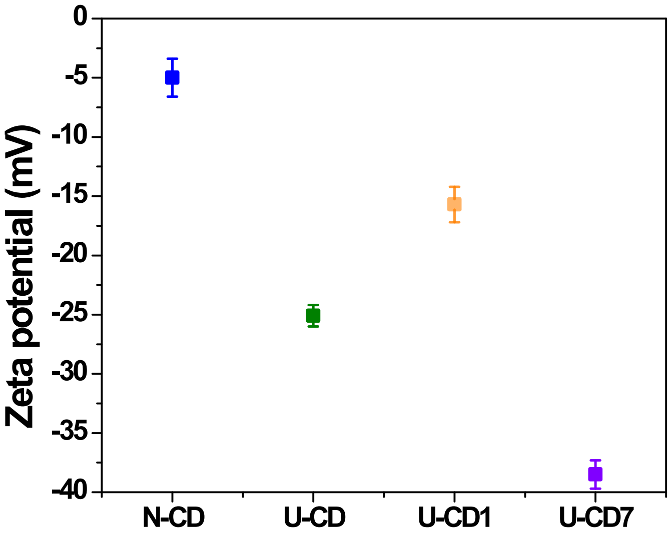

Figure S3. Zeta-potential of all CDs prepared in this study.

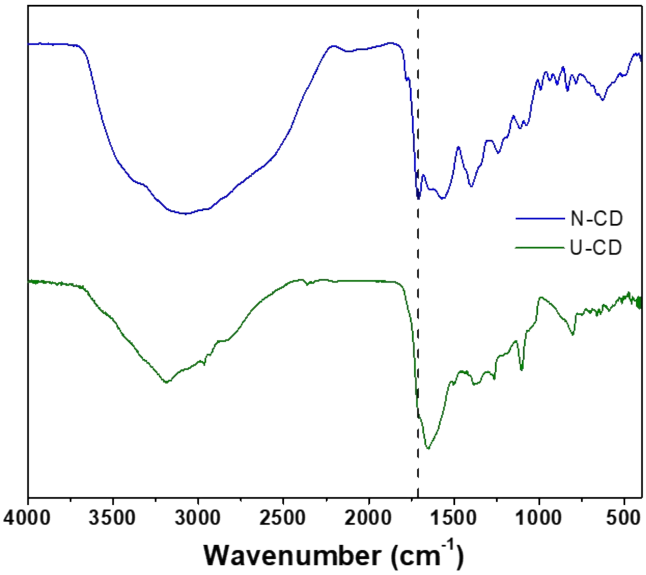

Figure S4. Fourier transform-infrared (FT-IR) spectra of the CDs. Dashed line represents the carboxylic acid group at 1709 cm^{-1}**.**

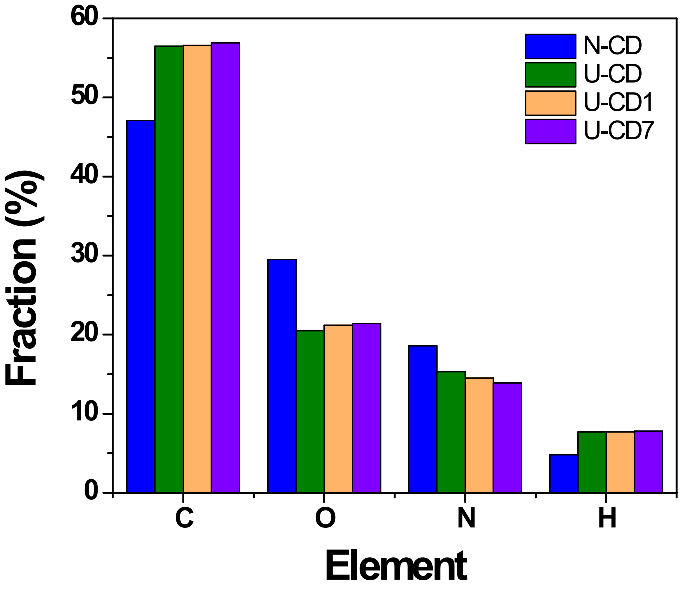

Figure S5. Elemental analysis results for all CDs prepared in this study.

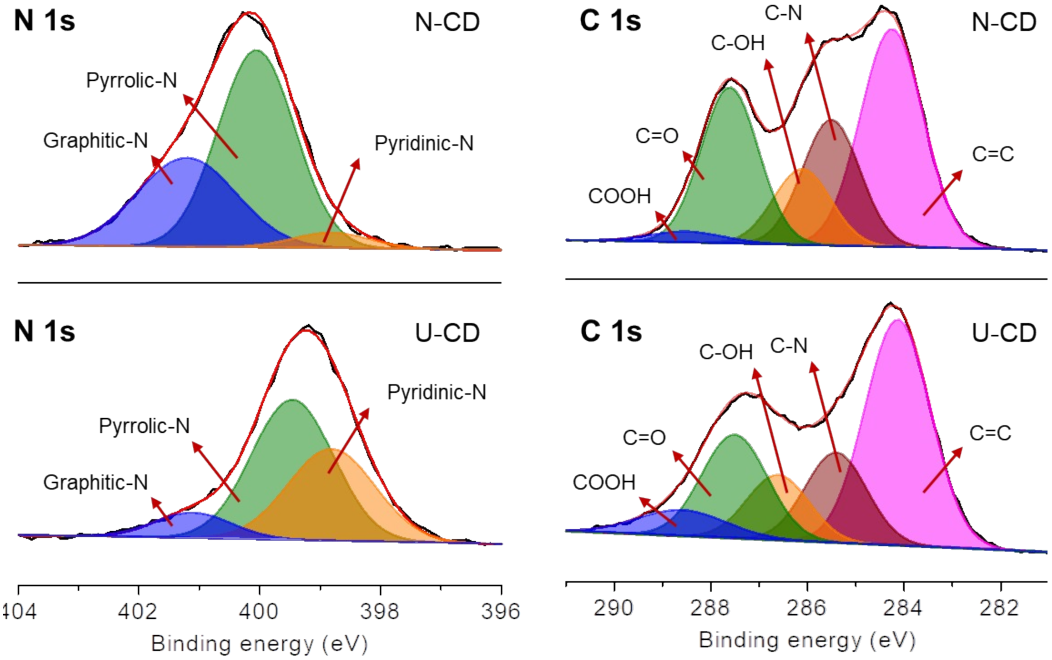

Figure S6. Deconvoluted C 1s and N 1s XPS spectra of the N-CD and U-CD.

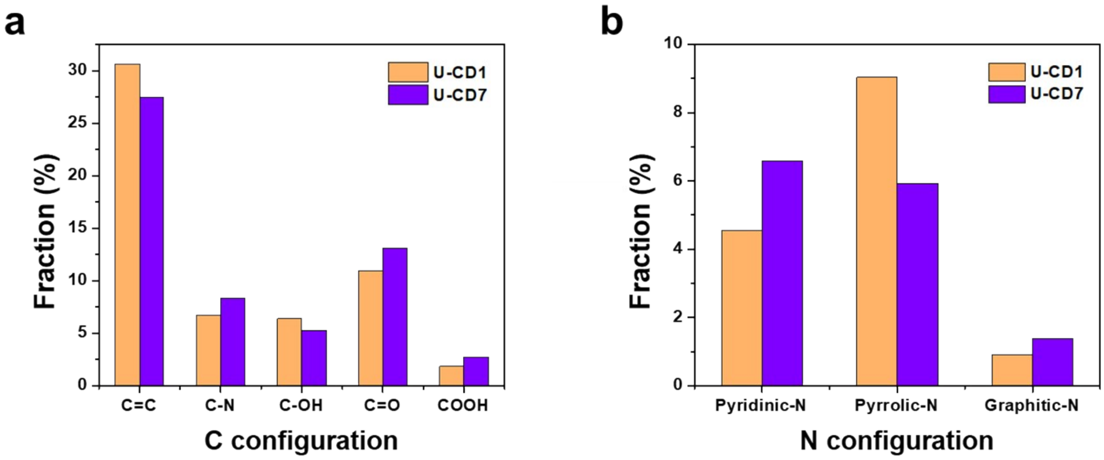

Figure S7. Chemical compositions of U-CD1 and U-CD7. The chemical compositions are determined by (a) high-resolution XPS spectra of C 1s and (b) N 1s, respectively.

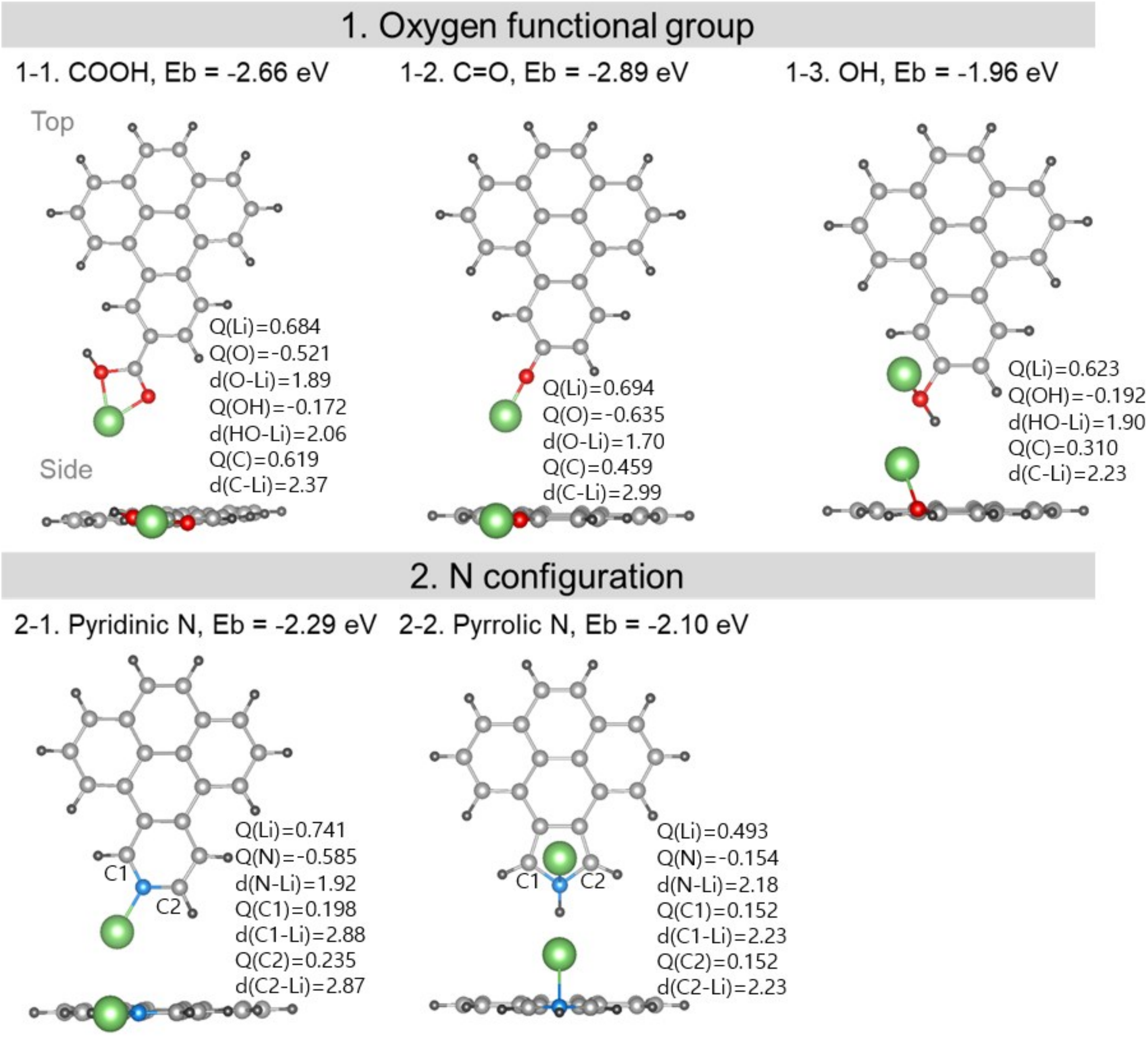

Figure S8. Model structures for the binding energy calculation of a Li ion with single functional groups.

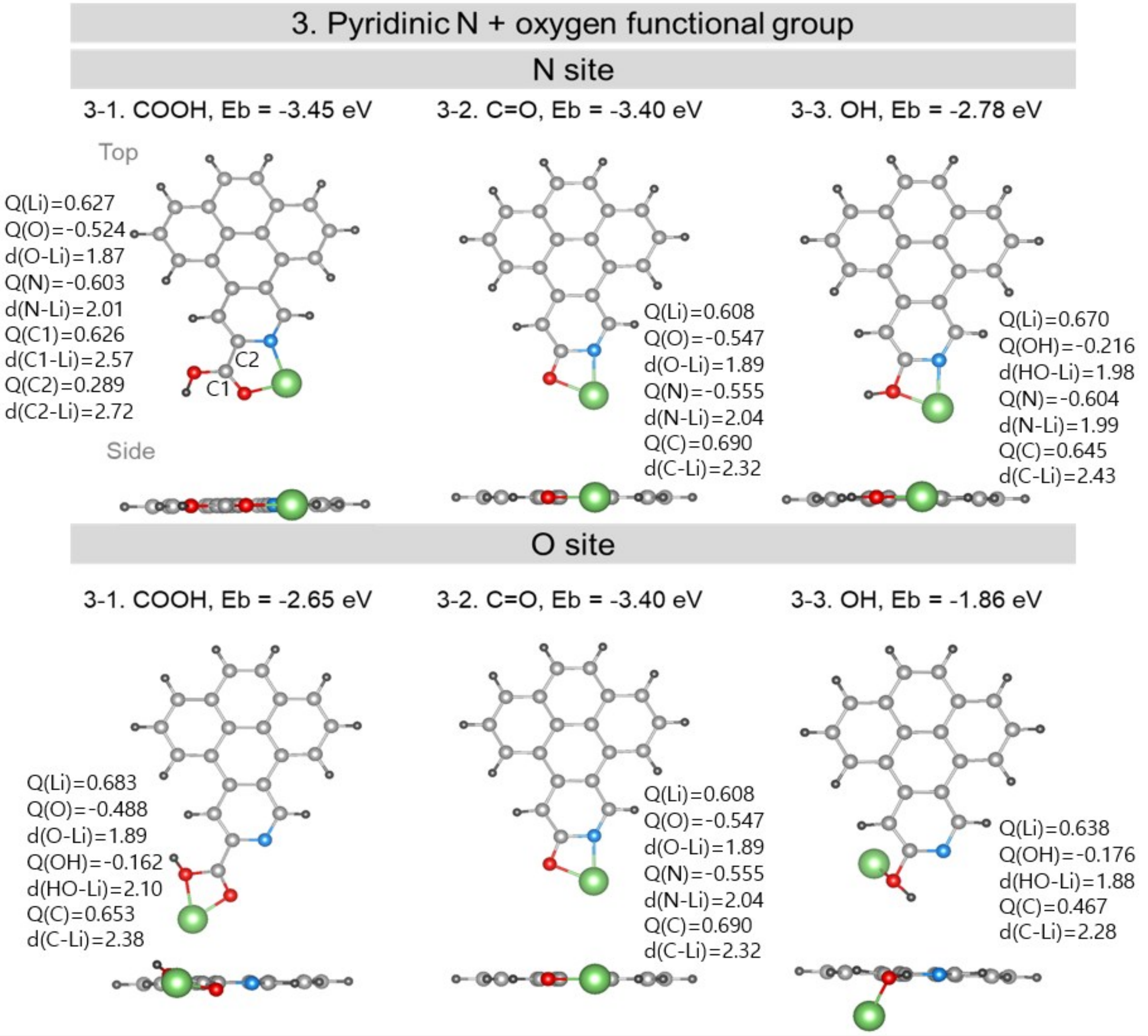

Figure S9. Model structures for the binding energy calculation of Li ion with two functional groups containing pyridinic-N.

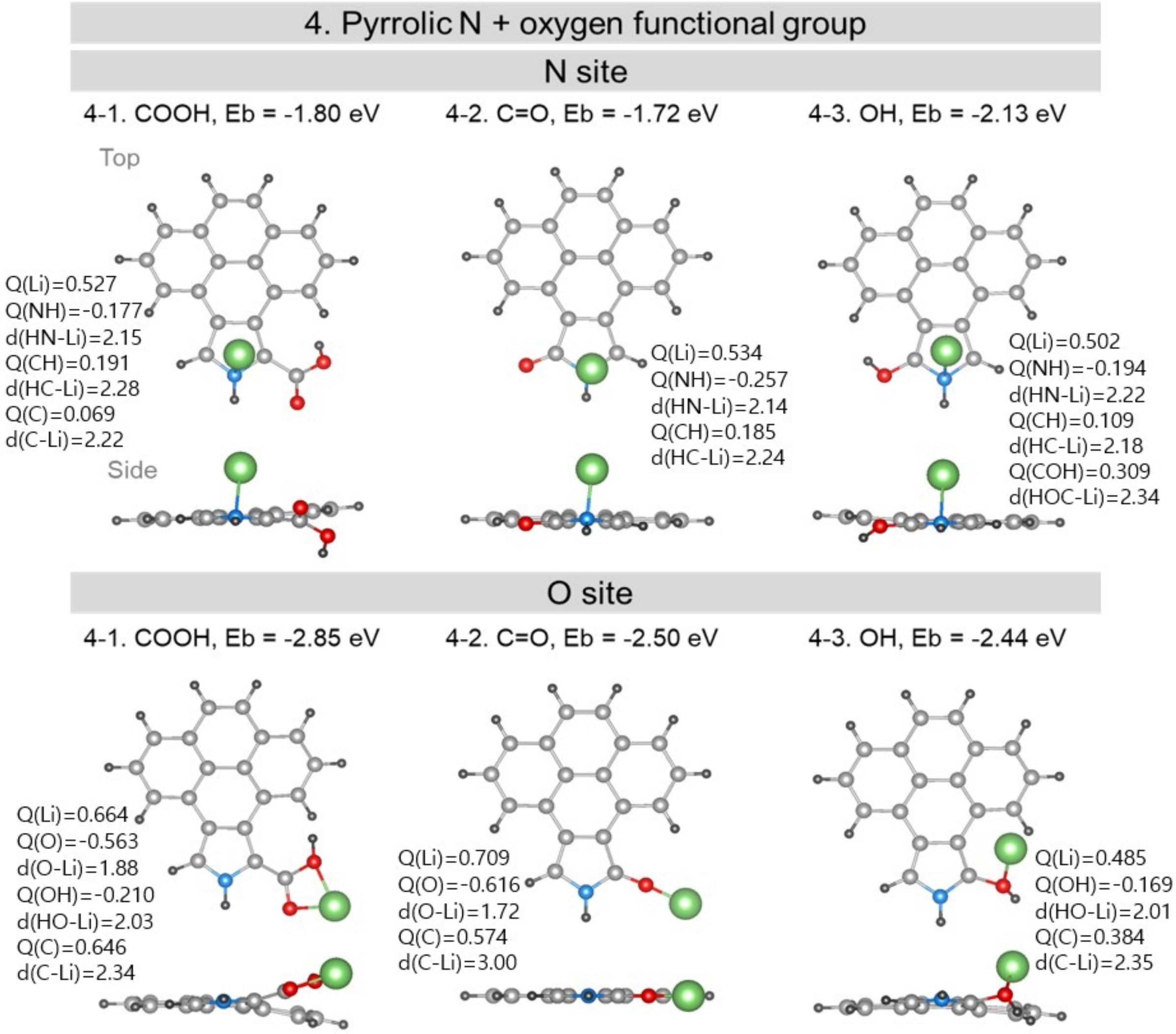

Figure S10. Model structures for the binding energy calculation of a Li ion and two functional groups containing pyrrolic-N.

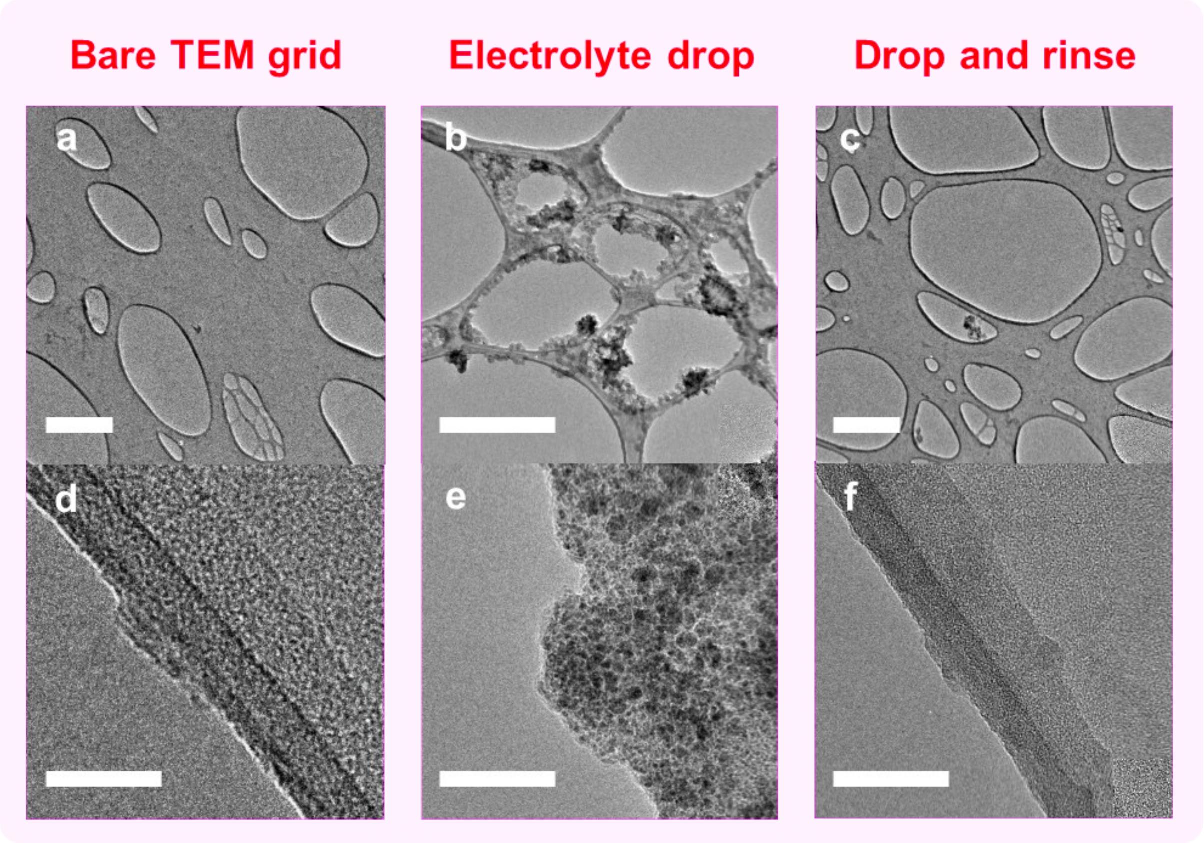

Figure S11. Series of TEM images of grid with various states. (a, d) Bare TEM grid. (b, e) U-CD-containing electrolyte dropped on a TEM grid exhibiting a messy grid surface and U-CD agglomeration. (c, f) U-CD-contained electrolyte dropped and rinsed TEM grid with the clean grid surface attributed to the weak adhesion of non-electrochemical adsorption. Scale bars are 1 μm (a–c); and 20 nm (d–f).

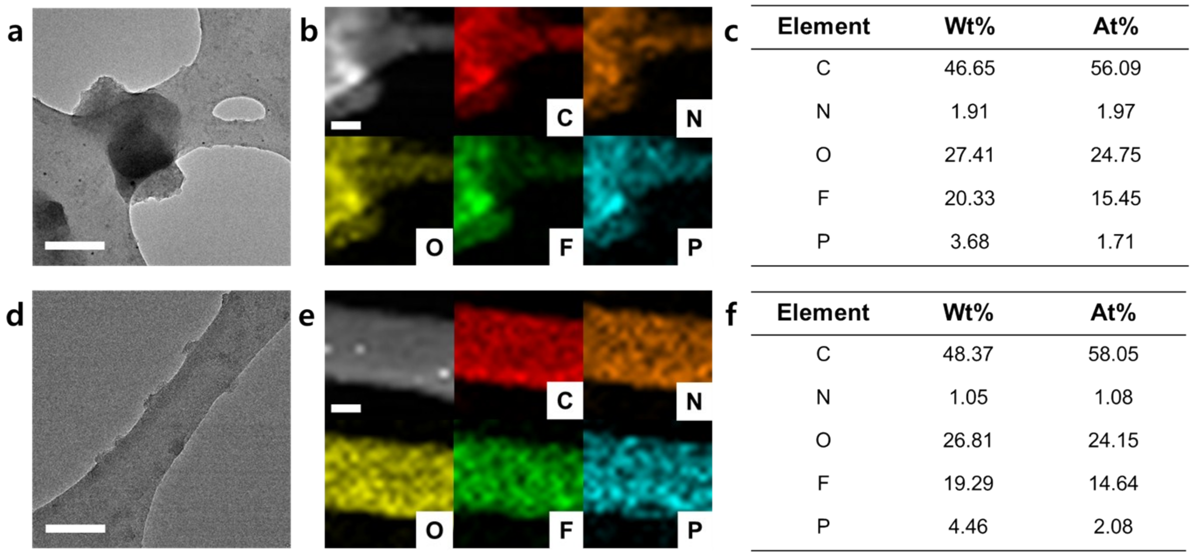

c

Element	Wt%	At%
C	46.65	56.09
N	1.91	1.97
O	27.41	24.75
F	20.33	15.45
P	3.68	1.71

f

Element	Wt%	At%
C	48.37	58.05
N	1.05	1.08
O	26.81	24.15
F	19.29	14.64
P	4.46	2.08

Figure S12. Series of TEM images of the U-CD-assisted Li plating/stripping behaviour at the initial stage, and the corresponding EDS analysis. U-CD-assisted Li plating/stripping of (a, d) TEM images; (b, e) element distribution; and (c, f) element contents, respectively. The nitrogen content is reduced after stripping. The U-CD concentration is 0.5 mg mL^{-1}. Scale bars are 100 nm (a, d) and 20 nm (b, e).

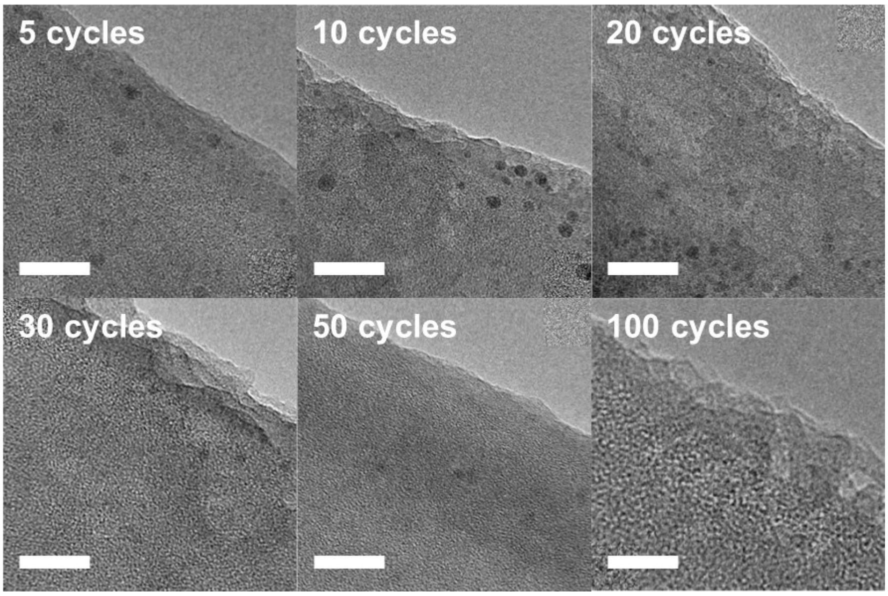

Figure S13. Series of TEM images of the U-CD-assisted plating after multiple cycles. The conditions of the electrochemical plating/stripping are a current density of 1 mA cm^{-2} with areal capacity of 1 mA h cm^{-2}. Scale bars are 20 nm.

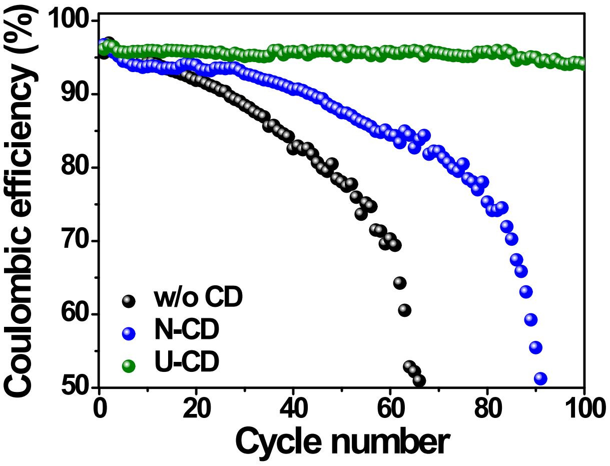

Figure S14. Cycle retention properties of the Li/Cu half-cell at 1C-rate with areal capacity of 1 mA h cm^{-2}. The electrolyte concentration is 0.5 mg mL^{-1}.

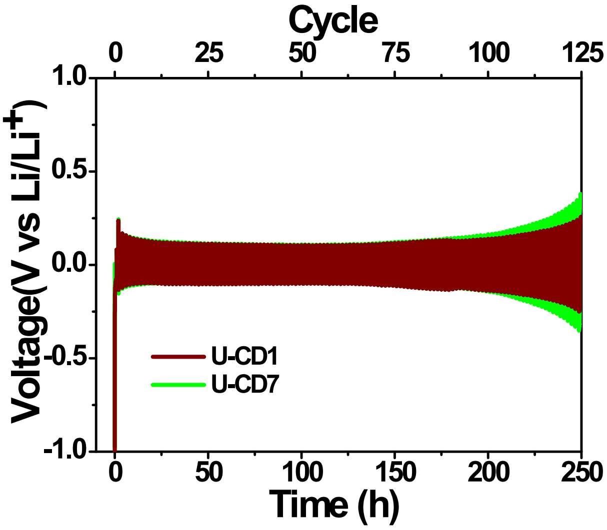

Figure S15. Electrochemical performances of the Li/Li symmetric-cell with U-CD functional group control. Cycle retention properties at 1C-rate with areal capacity of 1 mA h cm^{-2}. The electrolyte concentration is 0.5 mg mL^{-1}.

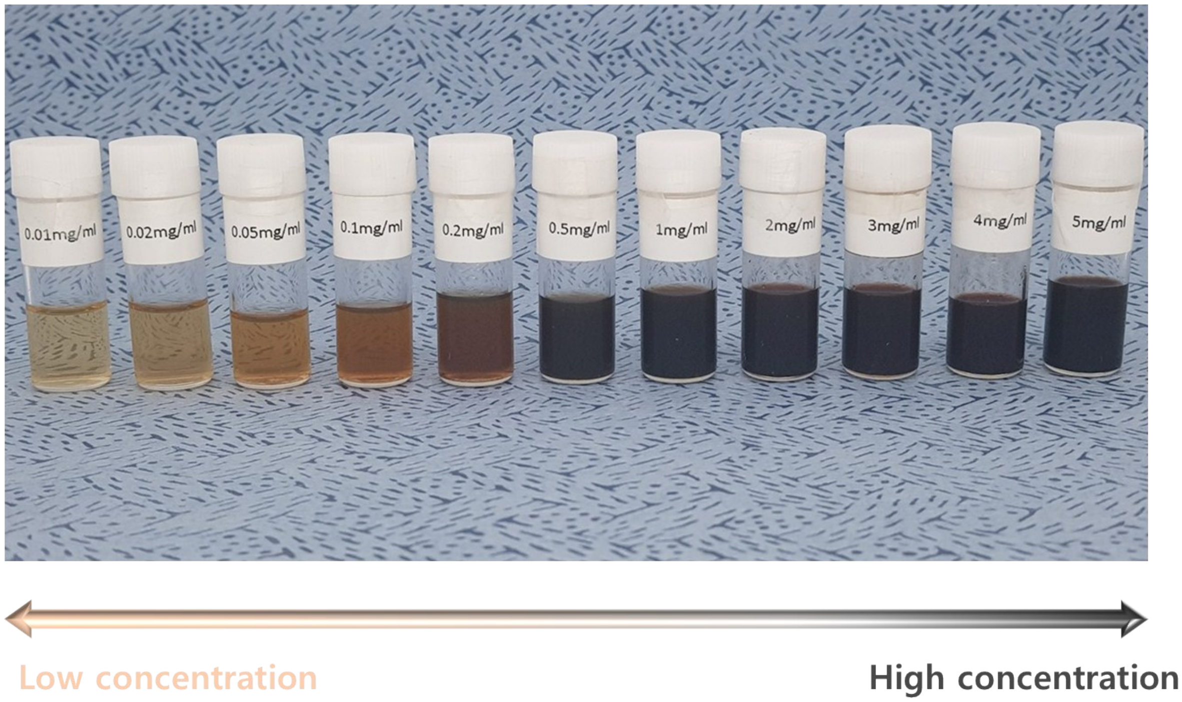

Figure S16. A photograph of the U-CD-dispersed electrolyte at different concentrations.

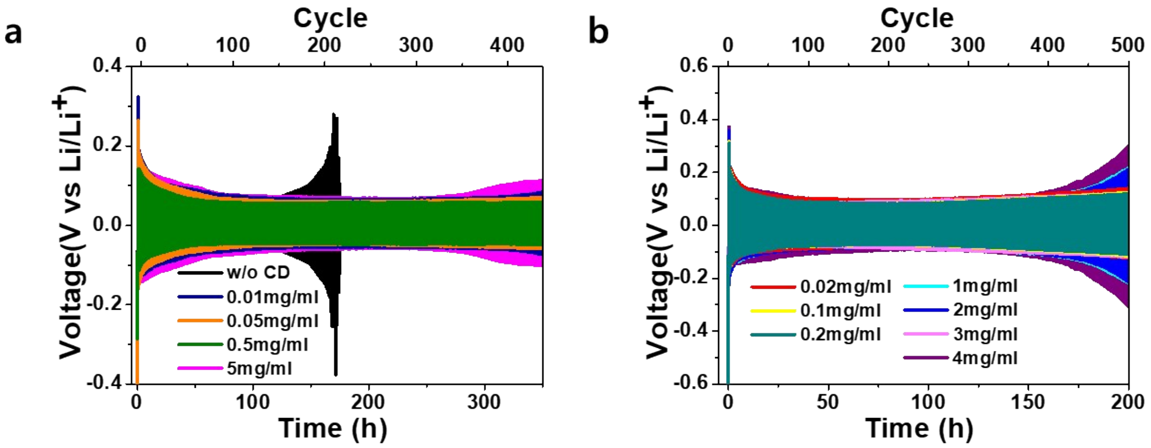

Figure S17. Electrochemical performances of the Li/Li symmetric-cell with various concentrations of U-CD dispersed electrolytes. Cycle retention properties of (a) 2.5 C-rate with areal capacity of 0.5 mA h cm^{-2} and (b) 5 C-rate with areal capacity of 0.5 mA h cm^{-2}.

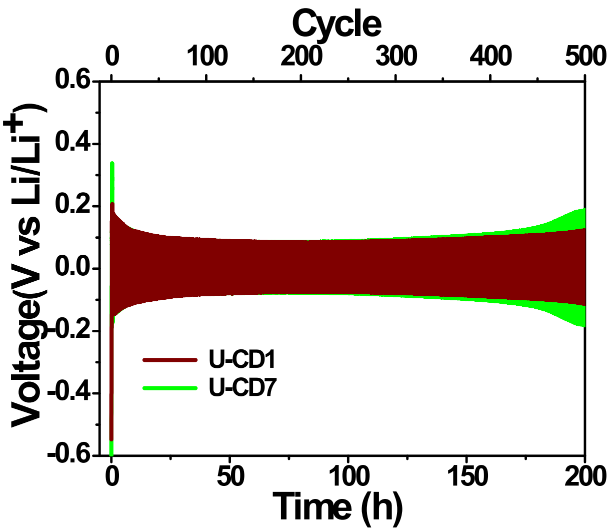

Figure S18. Electrochemical performances of the Li/Li symmetric-cell with U-CD functional group control. Cycle retention properties at 5C-rate with areal capacity of 0.5 mA h cm^{-2}. The electrolyte concentration is 0.5 mg mL^{-1}.

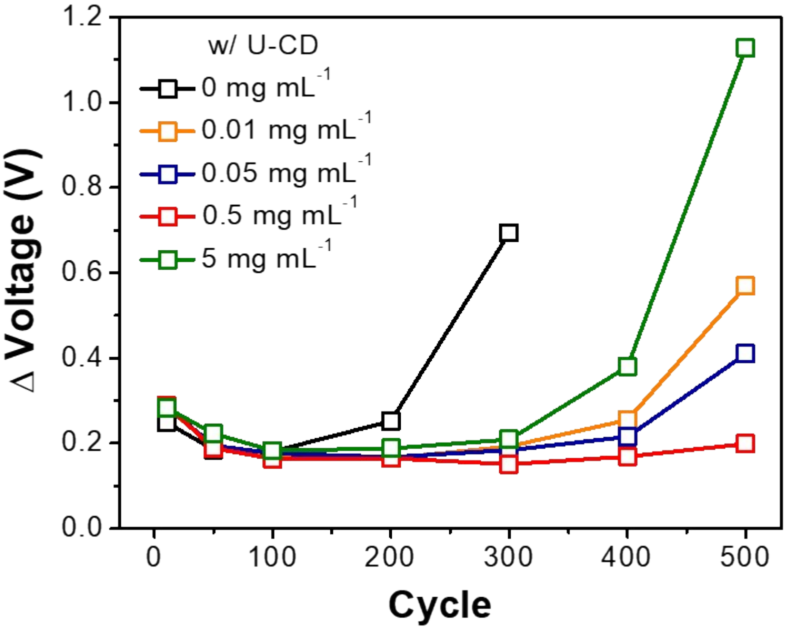

Figure S19. Plots of voltage differences of Li/Li symmetric-cell at a current density of 2.5mA cm^{-2} and an areal capacity of 0.5 mA h cm^{-2} with electrolyte concentration control.

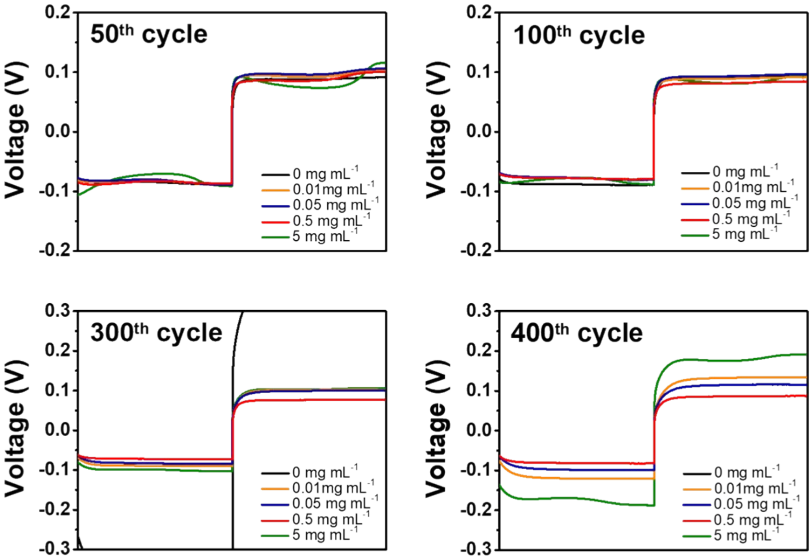

Figure S20. The magnified voltage profiles of Li/Li symmetric-cell corresponding with Figure. 3c at a specific cycle.

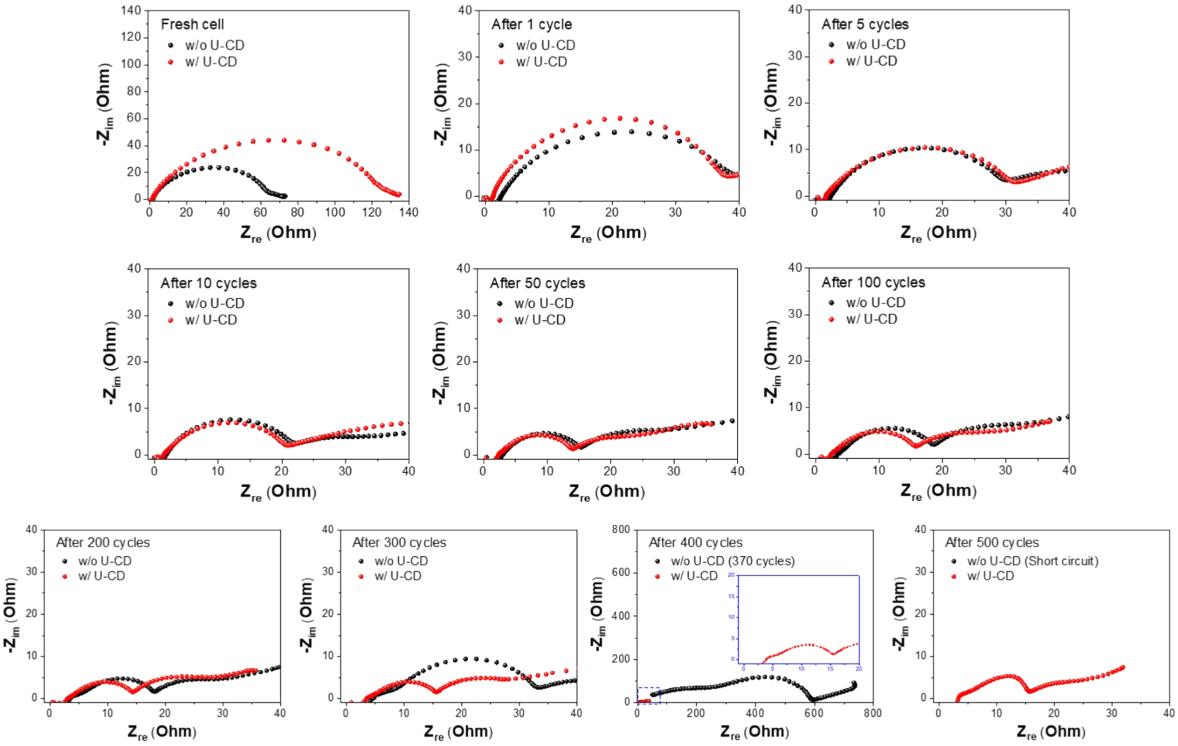

Figure S21. The impedance spectra behaviour after the number of cycles with and without U-CD.

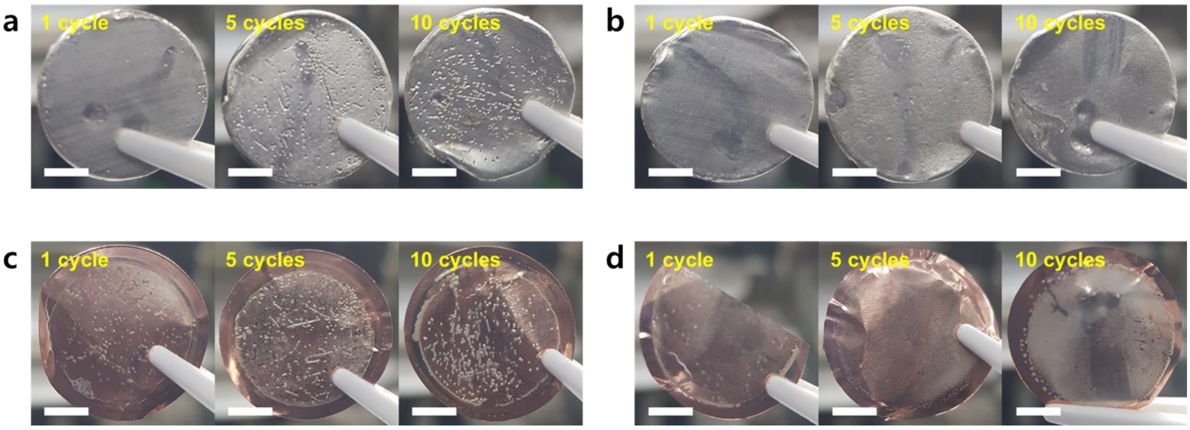

Figure S22. Series of photographs of the disassembled Li/Cu half-cell at the initial stage. (a) Li metal without the CD. (b) Li metal with the U-CD. (c) Li metal plated Cu foil without the CD. (d) Li metal plated Cu foil with the U-CD. The electrochemical test conditions are 1C-rate with areal capacity of 1 mA h cm^{-2}. Scale bars are 5 mm. The electrolyte concentration is 0.5 mg mL^{-1}.

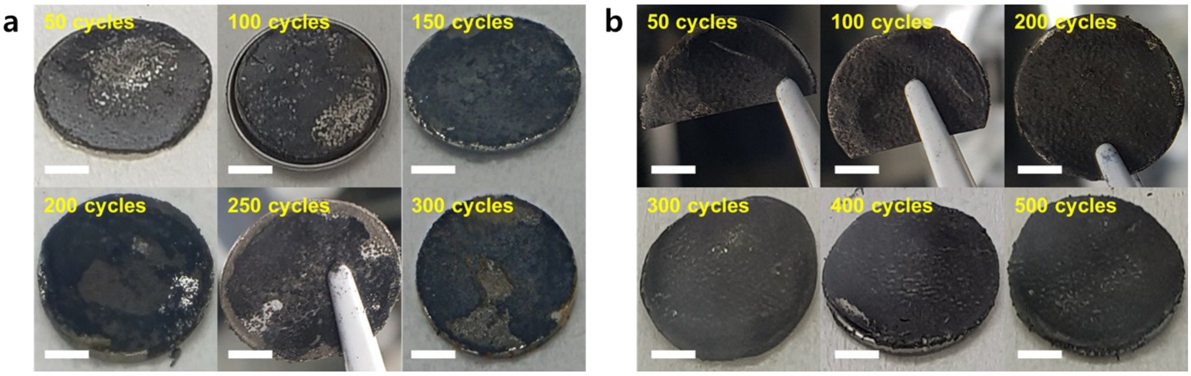

Figure S23. Series of photographs of the disassembled Li/Li symmetric-cell after numerous cycles. (a) Li metal without the CD. (b) Li metal with the U-CD. The electrochemical test conditions are 5C-rate with areal capacity of 0.5 mA h cm^{-2}. Scale bar is 5 mm. The electrolyte concentration is 0.5 mg mL^{-1}.

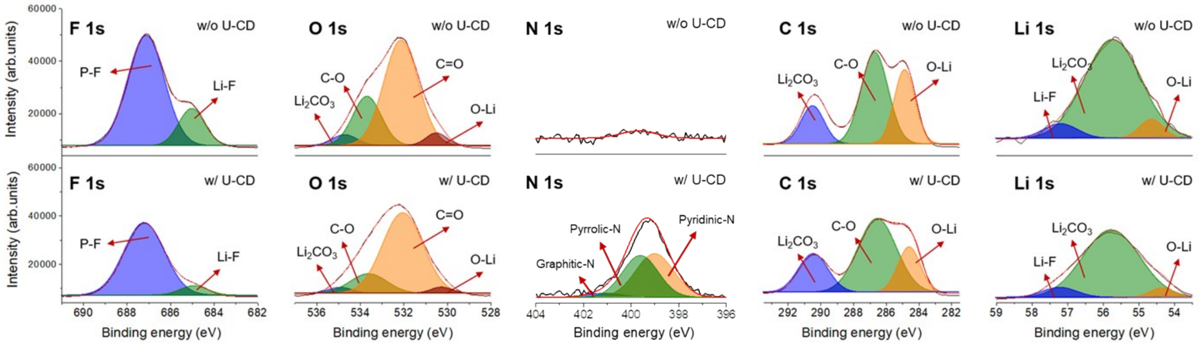

Figure S24. Chemical composition of the SEI produced after cycling Li metal determined by the high-resolution XPS spectra of F 1s, O 1s, C 1s, and Li 1s, respectively.

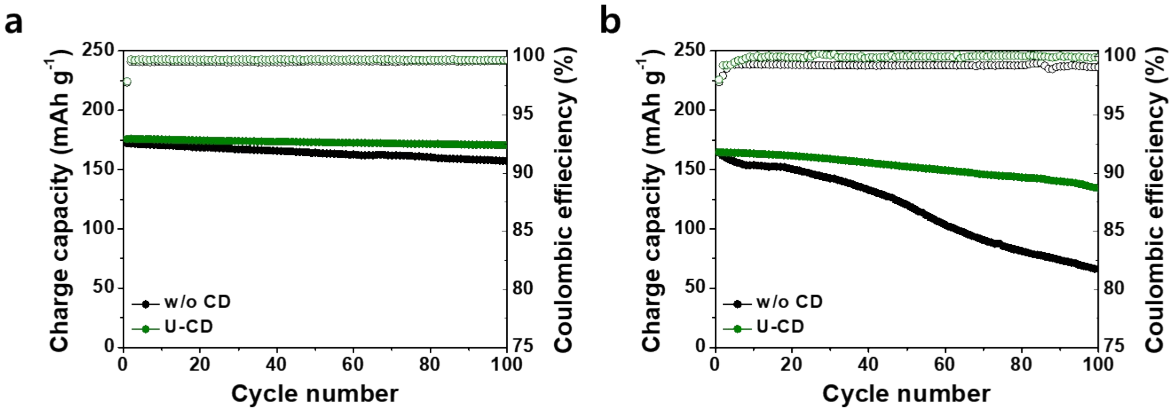

Figure S25. Cycle retention properties of the Li/LCO full-cell with 300 μm thickness Li. (a) 1C-rate with areal capacity of 1 mA h cm^{-2}. (b) 1C-rate with areal capacity of 3 mA h cm^{-2}.

Note S1. DFT assessment of the binding energy of a Li ion and the CD edge functional groups

The binding energy for the various types of edge functional groups is calculated with the structural models presented in **Figure S8–S10.** The main binding mechanism for the individual and hetero groups is described below.

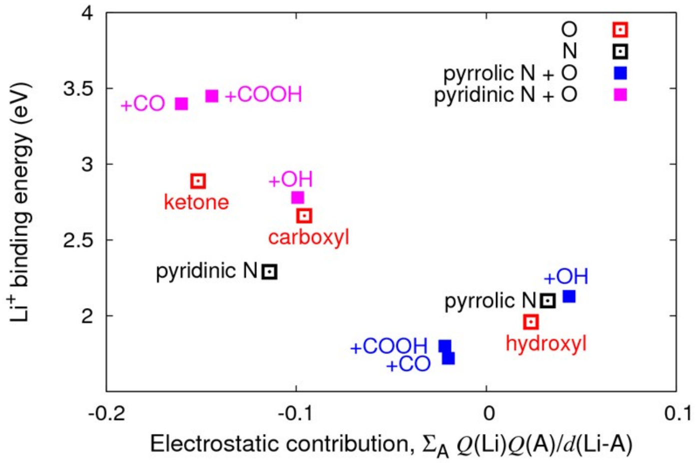

The contribution of the electrostatic attraction was extracted by summing the Coulomb energy contributed by all the atoms up to the second nearest neighbour (~3 A in distance) from the Li ion, i.e., $\sum_{A} Q(Li)Q(A)/d(Li-A)$, where Q(Li) or Q(A) is the Mulliken charge of the Li ion or its neighbour atom A with interatomic distance d(Li-A). The correlation between the calculated binding energy and electrostatic contribution is shown in the following figure. In case of the individual groups, the oxygen group (ketone, carboxyl, and hydroxyl) exhibits a larger variation in the binding energy with respect to the variation in the electrostatic contribution. This indicates a larger extent of the electrostatic interaction for the oxygen group than that for the nitrogen group. For the N groups, a significant role of the covalent-type interaction by the N lone pair is expected. However, the binding energy is significantly affected by the presence of another functional group nearby. For example, in the case of pyrrolic-N (blue filled squares), the binding energy is decreased by the neighbouring carboxyl or ketone group despite the enhanced electrostatic attraction, whereas the hydroxyl group slightly affects. The most probable reason is that the interaction between the Li ion and delocalised electron pair of the pyrrolic-N is largely disrupted by the COOH and C=O groups. In case of pyridinic-N, the electron pair is rather localised, and thus, a synergetic effect can be achieved by including an oxygen group that can attract the Li ion, which is shown by the pink filled squares in the following figure.

Note S2. Optimal conditions for the U-CD.

To determine the optimal conditions for the U-CD additives, we first tested a Li/Li symmetric-cell with 11 U-CD concentration variation samples (0.01 mg mL^{-1} to 5 mg mL^{-1}). We considered that dilute solutions did not function well owing to the lack of seeds and a high cell resistance of a thick sample. Similar to our assumption, the appropriate density of 0.5 mg mL^{-1} indicated excellent cycling. In addition, we examined the functional group modification effect of the U-CD with a fixed concentration of 0.5 mg mL^{-1}. We presupposed that the sample that had the strongest charge force and binding energy would show the best performance. However, according to the Li/Li symmetric cell-test, it seemed that excessive charges (U-CD7) hindered the deposition on the current collector by drawing Li ions to the drifting CDs, resulting in a cell resistance increase. In addition, the relatively weak negative charges of the U-CD1 functional group could not attract Li ions effectively, leading to insufficient battery performances. Therefore, among the U-CD variations, the U-CD that possessed adequate surface charge and strong Li ion attraction force exhibited excellent cyclability and minimum overpotentials.

Table S1. Calculated binding energy for Li ion and various functional groups.

NO.	Functional group	Binding energy (eV)
1-1	COOH	-2.66
1-2	C=O	-2.89
1-3	OH	-1.96
2-1	Pyridinic N	-2.29
2-2	Pyrrolic N	-2.10
3-1	Pyridinic N + COOH (N site)	-3.45
3-1	Pyridinic N + COOH (O site)	-2.65
3-2	Pyridinic N + C=O	-3.40
3-3	Pyridinic N + OH (N site)	-2.78
3-3	Pyridinic N + OH (O site)	-1.86
4-1	Pyrrolic N + COOH (N site)	-1.80
4-1	Pyrrolic N + COOH (O site)	-2.85
4-2	Pyrrolic N + C=O (N site)	-1.72
4-2	Pyrrolic N + C=O (O site)	-2.50
4-3	Pyrrolic N + OH (N site)	-2.13
4-3	Pyrrolic N + OH (O site)	-2.44

Table S2. Overpotential behaviour of the Li/Li symmetric cell with the various concentrations of U-CD during multiple cycles of cell operation.

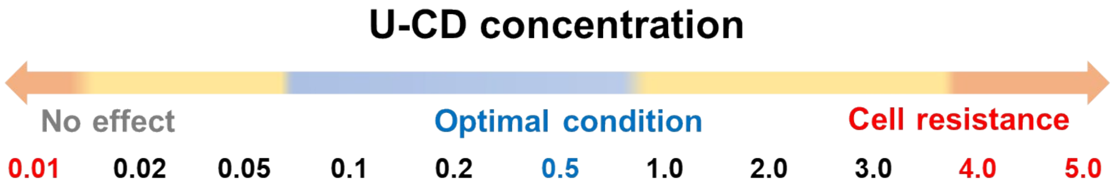

Cycle number Concentration	10th ΔV (V)	50th ΔV (V)	100th ΔV (V)	200th ΔV (V)	300th ΔV (V)	400th ΔV (V)	500th ΔV (V)
0 mg mL^{-1}	0.249	0.185	0.181	0.252	0.694	X	X
0.01 mg mL^{-1}	0.286	0.192	0.171	0.165	0.193	0.255	0.569
0.02 mg mL^{-1}	0.311	0.213	0.191	0.179	0.194	0.221	0.264
0.05 mg mL^{-1}	0.286	0.195	0.177	0.168	0.184	0.216	0.410
0.1 mg mL^{-1}	0.285	0.189	0.166	0.155	0.172	0.202	0.239
0.2 mg mL^{-1}	0.286	0.197	0.167	0.154	0.168	0.196	0.228
0.5 mg mL^{-1}	0.289	0.189	0.164	0.165	0.151	0.169	0.199
1.0 mg mL^{-1}	0.308	0.204	0.178	0.165	0.182	0.225	0.434
2.0 mg mL^{-1}	0.312	0.208	0.184	0.165	0.179	0.224	0.425
3.0 mg mL^{-1}	0.194	0.166	0.164	0.177	0.194	0.214	0.245
4.0 mg mL^{-1}	0.308	0.255	0.212	0.184	0.191	0.258	0.606
5.0 mg mL^{-1}	0.284	0.223	0.183	0.188	0.209	0.380	1.127